JOURNAL OF GEOPHYSICAL RESEARCH, VOL. 113, D00C04, doi:10.1029/2007JD009446, 2008

Aerosol optical thicknesses over North Africa: 1. Development of a product for model validation using Ozone Monitoring Instrument, Multiangle Imaging Spectroradiometer, and Aerosol Robotic Network

Sundar A. Christopher,[1] Pawan Gupta,[1] James Haywood,[2] and Glenn Greed[2]

Received 2 October 2007; revised 11 March 2008; accepted 28 March 2008; published 29 July 2008.

[1] Daily aerosol optical thickness (AOT) at 0.55 μm over the desert regions is needed as a source of validation for numerical models such as the United Kingdom's Numerical Weather Prediction Unified Model. We examined the relationship between monthly mean ultraviolet (UV) absorbing aerosol index (AI) from the Ozone Monitoring Instrument (OMI) that is available on a daily basis with the Multiangle Imaging Spectroradiometer (MISR) AOT that is available once every nine days over North Africa. We then developed spatiotemporal AI-AOT relationships on a monthly mean basis that can be used to convert the daily AI to AOT during months when dust concentrations are high (June–August) to compare against months when a mixture of dust and biomass burning aerosols are present (January–March). We further examined the AOT data from the ground to validate our methods and results. While previous studies have examined the Total Ozone Mapping Spectrometer AI with limited ground-based Sun photometer data, our study extends this to the OMI over 2 years (2005–2006) and for the entire north African region (20°W–40°E and 0–30°N). Our results confirm that the MISR is an excellent sensor for retrieving AOT over desert regions. Comparisons between MISR and Aerosol Robotic Network (AERONET) data over multiple locations indicate that the linear correlation coefficient is 0.89. The AI-AOT relationship is region specific and is robust over locations where AI and AOT are high during June–August especially when the predominant aerosol is dust. This relationship breaks down closer to the equator when aerosol loading is small especially when biomass-burning aerosols are prevalent during January–March. Our analysis indicates that the estimated AOT (EAOT) from the AI-AOT relationship is within 28% of the MISR AOT for optical depths between 0.2 and 2.0 with large uncertainties (75%) for smaller optical depths (<0.2). The EAOT for January–March 2006 is well correlated with the AERONET AOT with a linear correlation coefficient of 0.83 with a relative mean error of 23%. The methods and products developed here can be used as a first proxy for validating model-derived AOT that is shown by Greed et al. (2008).

Citation: Christopher, S. A., P. Gupta, J. Haywood, and G. Greed (2008), Aerosol optical thicknesses over North Africa: 1. Development of a product for model validation using Ozone Monitoring Instrument, Multiangle Imaging Spectroradiometer, and Aerosol Robotic Network, *J. Geophys. Res.*, *113*, D00C04, doi:10.1029/2007JD009446.

1. Introduction

[2] The role of aerosol effects on climate has gained renewed attention in the last decade since they change the radiation balance of the earth-atmosphere system by reflecting and absorbing solar radiation, modifying cloud properties and reducing the amount of solar radiation reaching the ground [*Intergovernmental Panel on Climate Change*, 2007]. The spatial and vertical distribution of aerosols and their absorptive and reflective properties also influence atmospheric circulation patterns, cloud formation and hydrological processes. Therefore, monitoring the spatial distribution of aerosols and their properties is critical for climate research, and for validating the performance of dust models in higher-resolution mesoscale models [*Haywood et al.*, 2005].

[3] Although several hundred Aerosol Robotic Network (AERONET) measurements are available around the world that routinely provide aerosol optical thickness (AOT) data [*Holben et al.*, 2001], satellite remote sensing provides far more complete global coverage. As part of the A-train, the newly launched Cloud Aerosol Lidar and

[1] Department of Atmospheric Sciences, University of Alabama in Huntsville, Huntsville, Alabama, USA.
[2] United Kingdom Meteorological Office, Devon, UK.

0148-0227/08/2007JD009446$09.00

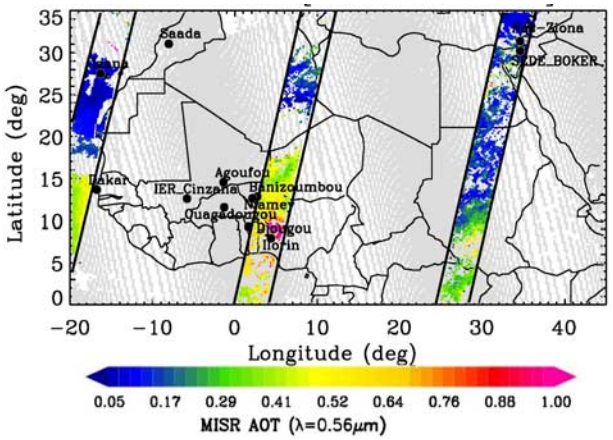

Figure 1. Area of study with OMI aerosol index values for 21 January 2006. Also superimposed are the MISR swaths in color with AERONET locations.

Infrared Pathfinder Satellite Observation (CALIPSO) and CloudSat satellites provide vertical profiling capabilities that will further improve our understanding of clouds and aerosols on the global climate system [*Stephens et al.*, 2005].

[4] Satellite remote sensing of aerosols has a rich heritage with retrievals of AOT from visible infrared sensors such as the Advanced Very High-Resolution Radiometer (AVHRR) [e.g., *Mishchenko et al.*, 2004] to ultraviolet (UV) indices and AOT from the Total Ozone Mapping Spectrometer (TOMS) [*Torres et al.*, 2002] and the Ozone Monitoring Instrument (OMI) [*Torres et al.*, 2007]. Considerable advances have also been made since the launch of the Terra and Aqua satellites from both the Multi Angle Imaging Spectroradiometer (MISR) [*Kahn et al.*, 2005] and the Moderate Resolution Imaging Spectroradiometer (MODIS) [*Remer et al.*, 2005].

[5] Africa is the largest source of dust [*Prospero et al.*, 2002] and biomass burning aerosols [*Andreae and Merlet*, 2001]. In Africa, dust storms are usually concentrated during the Northern hemisphere summer months while biomass burning is prevalent during the dry season – typically during August–October in the Southern hemisphere and during December–March in the Northern hemisphere. Several measurement campaigns have focused on studying dust aerosols during the summer months [*Tanré et al.*, 2003] or biomass burning events during the dry season [*Swap et al.*, 2003]. Dust aerosols can affect the radiation balance not only near the source [*Zhang and Christopher*, 2003; *Haywood et al.*, 2003] but far downwind in the Atlantic Ocean [*Christopher et al.*, 2003]. Closer to the equator in Africa, biomass burning is prevalent and fires are routinely observed from space [*Giglio et al.*, 2006] along with the transport of aerosols downwind of these regions that also affect the radiation balance. Recently, the Dust and Biomass Burning Experiment (DABEX) and the African Monsoon Multidisciplinary Analysis (AMMA) Special Observation Period (SOP) were conducted in January–February, 2006 in North Africa (J. Haywood et al., Overview of the dust and biomass-burning experiment and African Monsoon Multidisciplinary Analysis special observation period, submitted to *Journal of Geophysical Research*, 2008) when both dust and biomass burning aerosols were present; this is one of the focus periods of this study.

[6] Our goal is to obtain the spatial distribution of aerosols over the Saharan desert with OMI and MISR satellite retrievals and validate our results with the AERONET data. The satellite data set is a useful constraint on numerical weather prediction models that require validation sources on aerosol spatial distribution and concentrations on a daily basis [*Haywood et al.*, 2005; *Greed et al.*, 2008]. At the time of analysis and writing, MODIS retrievals of AOT are not available over desert regions although recent versions include the MODIS Deep Blue AOT over bright targets [*Hsu et al.*, 2006]. The TOMS/OMI provides Aerosol Index (AI) values that are useful for separating absorbing from nonabsorbing aerosols in the UV part of the electromagnetic spectrum and has been widely used for tracking dust aerosols over North Africa [e.g., *Prospero et al.*, 2002]. AOT at 380 nm is also reported from the NIMBUS 7 TOMS and the EP TOMS instruments [*Torres et al.*, 2002]. More recently OMI data has also been used to report AOT at 0.50 μm that is in various stages of validation [*Torres et al.*, 2007]. However, our goal is to obtain AOT at 0.55 μm, a product that is available from MISR that compares well with AERONET data over deserts [*Kahn et al.*, 2005; *Wang et al.*, 2004].

[7] The MISR data does not provide daily coverage over the area of study (Figure 1) necessitating the use of OMI-MISR intercomparions. Previous studies have used the relationship between the TOMS AI and AERONET AOT over selected AERONET locations to derive AI-AOT relationships [*Hsu et al.*, 2000; *Haywood et al.*, 2005]. *Hsu et al.* [2000] used two AERONET locations in Africa, one in South America, and six in Africa for examining the AI versus UV AOT relationship. Their results showed that a linear relationship exists between AI and AOT indicating that the AI could be used as a surrogate for obtaining AOT. However, this relationship is dependent upon the aerosol type, the aerosol height and is also region specific. *Haywood et al.* [2005] used a similar approach to obtain AI-AOT relationship in July 2003 from two sites dominated by dust (Cape Verde and Dakar) and used this relationship to convert the AI to AOT over North Africa (10°N–40°N, 20°W–30°E). In this paper we examine the OMI AI versus MISR AOT relationship for 2 years (2005–2006) from a satellite perspective rather than using the AERONET data sets since the AERONET measurements are representative of point locations and are limited in spatial coverage. This is a complementary method to the newer aerosol products currently available from the MODIS deep blue, and OMI over desert regions.

[8] The paper is organized as follows. In section 2, we briefly describe the data and methods used. In section 3, we present the MISR-AERONET comparisons to test the MISR aerosol retrieval over desert areas, followed by the AI-AOT relationships that are then used to estimate AOT (EAOT). We complete the analysis by comparing the EAOT with the AERONET.

2. Data and Methods

[9] The area of study is shown in Figure 1 with the AERONET locations used along with complete swaths of

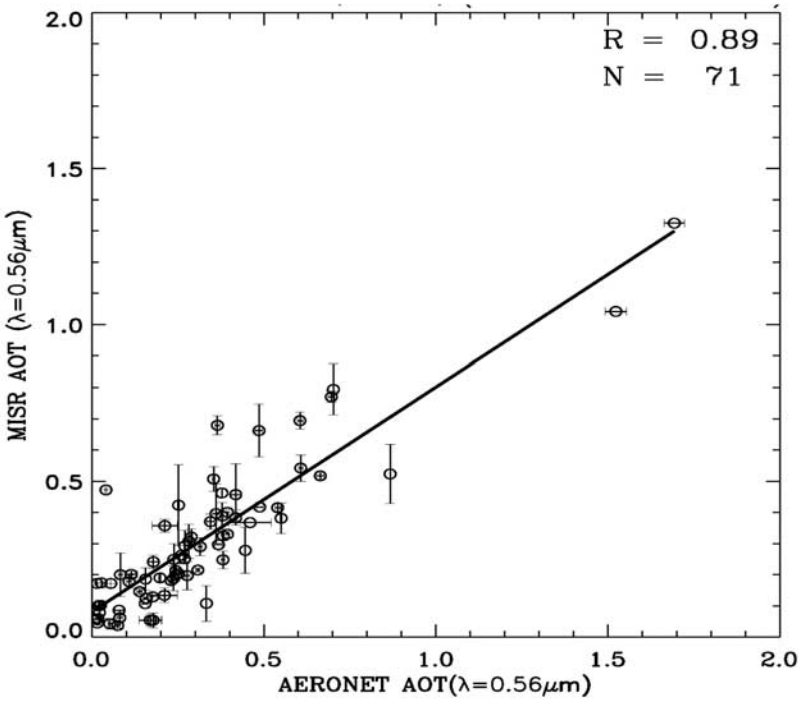

Figure 2. MISR versus hourly mean AERONET AOT for January–March 2006 for locations shown in Figure 1.

the OMI and MISR for 21 January 2006. The study region is between 20°W–40°E and 0–30°N. The data sets used in this study include total column AOT retrieved from the Terra-MISR, AI from OMI, and hourly AOT from the AERONET. A complete list of all data sets used is shown in Table 1.

2.1. MISR Aerosol Optical Thickness Data

[10] The MISR has four spectral channels (446, 558, 672, and 867 nm) with a spatial resolution of about 250 m to 1.1 km with nine cameras that enable aerosol retrievals globally without any limitations caused by surface type [*Kahn et al.*, 2005]. The spatial resolution of the level 2 aerosol product (MIL2ASAE, F09, 18) is 17.6X17.6 km^2 that was used for intercomparisons with the AERONET data. The expected uncertainty in this product is ±0.05 for AOT < 0.5 and ±10% for AOT > 0.5 [*Martonchik et al.*, 1998]. The MISR science team has performed comprehensive comparisons of the MISR AOT with the AERONET AOT globally from December 2000 to November 2002, and the results indicate that 63% of the MISR AOT values fall within 0.05 or 20% of AERONET AOT, and about 40% are within 0.03 or 10% of AERONET AOT [*Kahn et al.*, 2005]. The MISR L3 monthly mean AOT data are reported in a rectangular grid of 0.5° × 0.5° globally and is used for intercomparisons with the AI values (Table 1).

2.2. OMI Aerosol Index

[11] The OMI measures the upwelling radiance in the 270–500 nm bands. It has near daily global coverage with a 2600 km swath width and a spatial resolution of 13X24 km^{2}at nadir and 28 × 150 km^2 near the edge. The AI is derived from the difference between the wavelength dependence (354 and 388 nm) of reflected radiation in an atmosphere containing aerosols and a pure molecular atmosphere (Rayleigh scattering) [*Torres et al.*, 2007]. In the UV, absorbing aerosols such as dust and smoke often produce positive AI values. The AI values can also be inverted to produce UV AOT values that are highly dependent on assumptions in aerosol height leading to an overall uncertainty of about 30% in the retrieved AOT [*Torres et al.*, 1998]. Moreover the AI is not sensitive to boundary layer aerosols below 1–2 km and subpixel cloud contamination also poses problems [*Torres et al.*, 2005].

Table 1. List of Data Sets, Time Periods, and Their Resolution Used in the Study

Number	Satellite Sensor	Data Level	Period	Resolution	Data Set Name/Version
1	OMI AI	Level 2	January–March 2005, January–March 2006, June–August 2005	13 × 24 km, 0.5° × 0.5°	OMI AI
2	MISR AOT	Level 3	January–March 2005, January–March 2006, June–August 2005	0.5° × 0.5°	CGAS, F02, 14
3	MISR AOT	Level 2	January–March 2006	17.6 × 17.6 km^2	MIL2ASAE, F09, version 18
4	AERONET	Level 1.5	January–March 2006	Point	Direct Sun Algorithm, Version 2

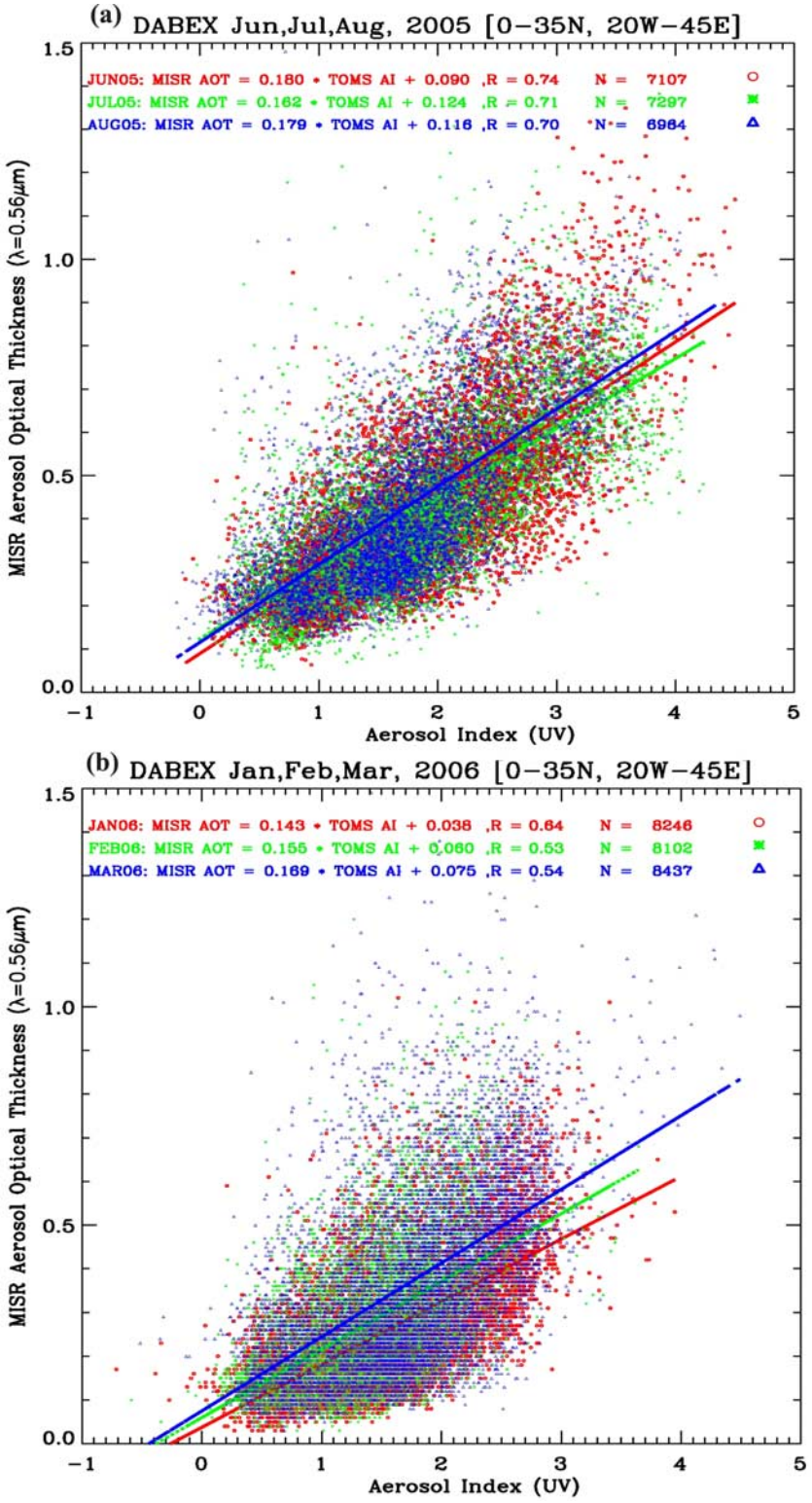

Figure 3. OMI aerosol index versus MISR AOT for 0.5° × 0.5° grids for (a) June–August 2005 and (b) January–February 2006.

[12] A previous version of manuscript used the EP-TOMS level 3 monthly mean AI data sets for January–March 2001–2004 and June–August 2000–2004. The EP-TOMS AI from 2000 had some errors due to calibration [*Kiss et al.*, 2007] and therefore we did not use the TOMS AI data. Table 1 provides a summary of the data sets used and the corresponding time periods.

2.3. AERONET Aerosol Optical Thickness Data

[13] The AERONET is a federation of well calibrated ground based Sun photometers that provide spectral AOT

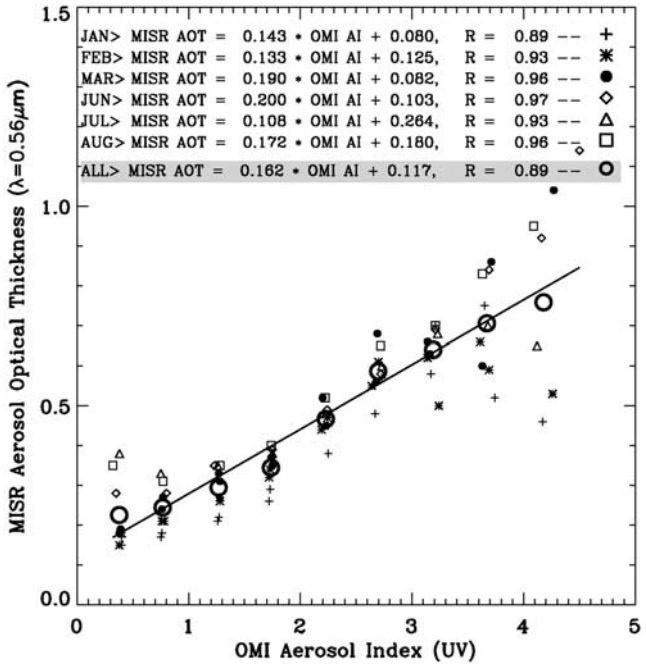

Figure 4. Bin-averaged relationship between OMI aerosol index and MISR AOT from 2005 to 2006 for each month. The slopes, intercepts, and correlation coefficients are also shown in the inset.

and other aerosol properties from hundreds of locations around the world [*Holben et al.*, 2001]. The hourly cloud-cleared level 1.5 data was used from 12 stations for 2006 (Figure 1) since the level 2.0 was not available during the time of analysis. The estimated uncertainty in AERONET AOT is about ±0.015 [*Dubovik and King*, 2000]. The AERONET data were compared against the MISR AOT values for January–March 2006. It is not the purpose of this paper to perform comprehensive multiyear MISR-AERONET comparisons since it is being accomplished by the MISR science team. We simply checked the MISR-AERONET comparisons during January–March 2006 since it coincided with the DABEX.

3. Results

[14] Figure 1 is the study area with OMI and MISR data superimposed for 21 January 2006 where the UK Met Office BAe 146 aircraft made aerosol measurements in and around Niamey during DABEX (J. Haywood et al., submitted manuscript, 2008). Three strips denoted in color show the MISR swaths on 21 January 2006 from the Terra overpass. Each strip is about 360 km wide and the shaded area inside the strips in gray shows valid MISR AOT pixels during that specific orbit. The relatively light shade shows the wide swaths of the OMI during the Aura overpass. Note that the MISR on Terra is on a descending mode with a local equatorial crossing time of 1030 UT whereas the OMI on Aura has a local equatorial crossing time of 1337 UT. Therefore differences are to be expected in the aerosol features that are sampled during these 3 h. Figure 1 indicates the advantage of the OMI over the MISR in terms of spatial coverage on any given day.

[15] The results are divided into several sections. Section 3.1 will discuss the MISR-AERONET intercomparisons. Section 3.2 will compare MISR AOT with the OMI AI; section 3.3 will provide a statistical analysis between the AI-AOT in $10^\circ \times 10^\circ$ latitude-longitude grids for 7 years; section 3.4 will discuss the OMI AOT estimations from the AI-AOT relationship (EAOT) and section 3.5 will compare the level 1.5 AERONET AOT with the EAOT.

3.1. MISR-AERONET Comparisons

[16] Figure 2 shows a scatterplot between AERONET and MISR AOT during January–March 2006 over several AERONET locations in the study area (Figure 1). The correlation is high (linear correlation coefficient (r) of 0.89, standard error of estimate (see) = 0.08, N = 71) indicating the high quality of the MISR aerosol product over desert regions. These results are consistent with MISR validation efforts from other desert locations [e.g., *Kahn et al.*, 2005; *Christopher and Wang*, 2004] and using the level 2 cloud-screened AERONET data may further improve these results.

3.2. Relationship Between MISR AOT and OMI AI

[17] One of the goals of this paper is to examine whether the AI can be used as a surrogate for AOT. To accomplish this task, we developed spatiotemporal relationships between the MISR AOT and AI that can be used to estimate AOT from the OMI AI values. The MISR AOT represents loading of all aerosol types in the entire atmospheric column whereas the AI is primarily sensitive to smoke and dust and is also sensitive to the height of aerosol layer [*Mahowald and Dufresne*, 2004; *Torres et al.*, 2005]. While the MISR AOT retrievals are less dependent on aerosol layer height, the dependence of AI on aerosol height is almost linear [*Torres et al.*, 1998; *Herman et al.*, 1997] and as the height of the aerosol layer increases, the AI values also increases [*de Graaf et al.*, 2005].

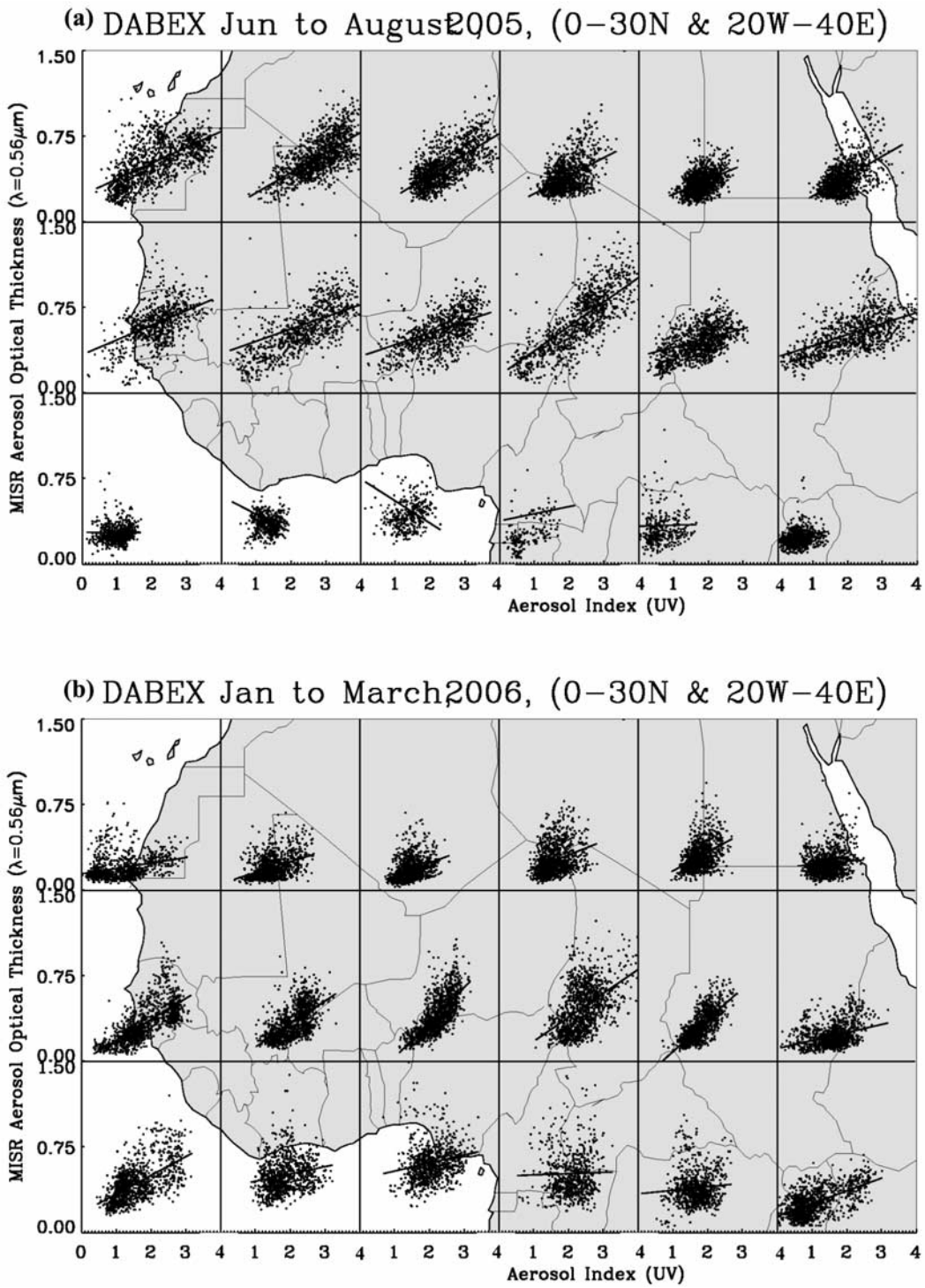

Figure 5. Scatterplot of OMI AI versus MISR AOT for 10° × 10° grid boxes for (a) June–August 2005 and (b) January–March 2006.

[18] The next step is to examine how well the MISR AOT compares with the OMI AI over the entire region of study. We selected two seasons, summer (June–August (JJA)) and spring (January–March (JFM)) since dust is predominant during JJA [*Greed et al.*, 2008] and a mixture of biomass burning and dust is prevalent during JFM (J. Haywood et al., submitted manuscript, 2008). Although 2 years of data were analyzed (2005–2006), we use JJA (2005) and JFM (2006) data to outline the results, while providing tables for other values. Figure 3 shows the relationship between monthly mean OMI and MISR data for the entire study area for JJA 2005 (Figure 3a) and for JFM 2006 (Figure 3b). The regression lines calculated for each month are also shown. The AI and AOT that are different measures of

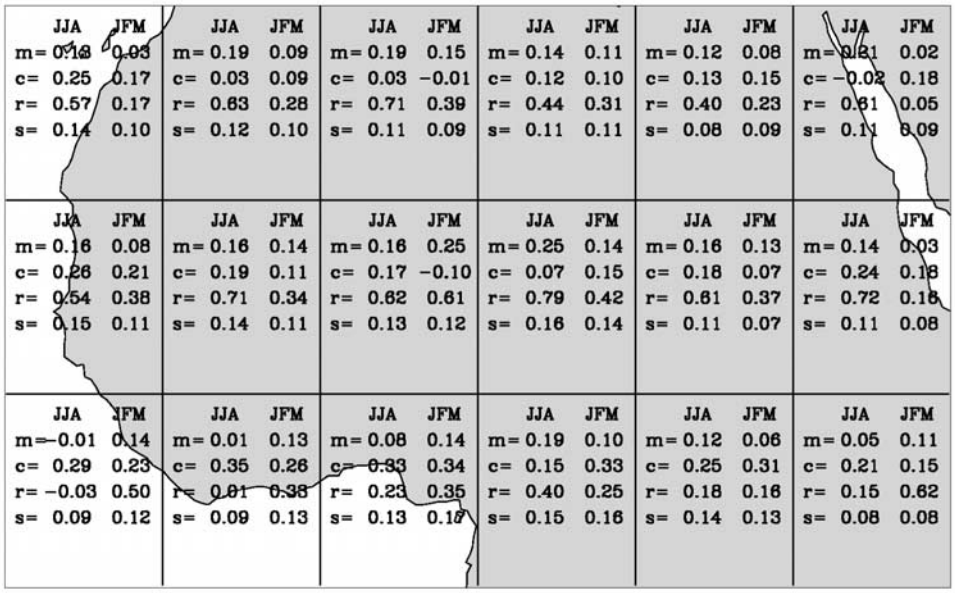

Figure 6. Slope (m), intercept (c), standard error estimate (s), and correlation coefficients (r) over each $10^\circ \times 10^\circ$ latitude-longitude box for summer (JJA) and spring (JFM).

aerosol loading show a linear relationship but with a large scatter that is similar to the results shown by *Haywood et al.* [2005]. Low sampling by the MISR as compared to the OMI could be one the reasons for large scatter combined with the difference in the overpass time. Also, there are several grid points in Figure 3, where MISR denotes very high AOT values when the AI is low. This could be due to several reasons including (1) monthly averaging of a large number of AI observations when MISR has fewer observations with higher aerosol loading; (2) the dependence of AI-AOT relationship on other factors such as aerosol type, aerosol concentrations, and local meteorology and; (3) possible cloud contamination in both MISR and OMI products [*Hsu et al.*, 1999].

[19] The linear correlation coefficient from our study over the different years varies from 0.53 to 0.64 for JFM and from 0.70 to 0.74 for JJA. The correlation during JJA is usually higher when compared to JFM probably due to aerosol heights and concentrations being higher during the summer months [*Hsu et al.*, 1999]. Previous studies that estimate the dust layer height using radiosonde data over Saharan region suggests values between 0.5 to 3 km during winter-spring months and it varies from 1.5 to 5.5 km during the summer months [*Hsu et al.*, 1999]. These values are reasonably consistent with the dust storms investigated during DABEX and the Dust Outflow and Deposition to the Ocean (DODO2) [*Osborne et al.*, 2008; *Greed et al.*, 2008]. The Lidar In-space Technology Experiment (LITE) measurements also show that Saharan dust layer height remains low during winter-spring months when compared to the summer months.

[20] To check the consistency of this linear relationship over 2 years, further analysis using bin averaged data was conducted (Figure 4). Figure 4 presents data for January–March from 2005 to 2006 and from June to August 2005. The AOT are averaged according to AI values (bins of 0.5) for each month for all the years where the different symbols represent different months. The AI-AOT relationship has high correlations with linear correlation coefficients varying from 0.89 to 0.97. The average slope and intercept are 0.16 and 0.12 respectively. Furthermore, the average slope (0.16) remains the same for summer and spring months whereas the intercept decreases from summer (0.18) to spring (0.10). The slope values are more consistent when compared to the intercept that varies significantly from season to season. The change in slope and intercept is possibly due to changes in aerosol type and height of the aerosol layer over the different seasons [*Hsu et al.*, 1999].

3.3. Regression Analysis as Function of Latitude-Longitude Grids

[21] To examine the spatial variation of the AI-AOT relationship, we divided the entire study area into $10^\circ \times 10^\circ$ latitude and longitude grids and analysis is performed for each grid box separately. Figure 5 shows AI-AOT relationship for JJA 2005 (Figure 5a) and for JFM 2006 (Figure 5b). To facilitate discussion, the study area is divided into three latitude belts, 0–10°N is lower-latitude belt (LLB), 10–20°N is mid latitude belt (MLB), and 20–30°N is upper latitude belt (ULB). During both seasons, there is more scatter in the AI-AOT relationship in the LLB when compared to the ULB. The AOT values are higher in the LLB during JFM since biomass burning is more prevalent during this time where as high AOTs are seen during JJA in the MLB and ULB, primarily because of dust aerosols. Also, there are significant differences in the AI-AOT relationship between the seasons since aerosol types, properties and the associated meteorology is different. Several $10^\circ \times 10^\circ$ grids in the LLB have land-ocean mixtures with combinations of smoke, dust and sea salt aerosols with weak AI-AOT relationships. The MLB is mostly dominated by dust during the summer months with

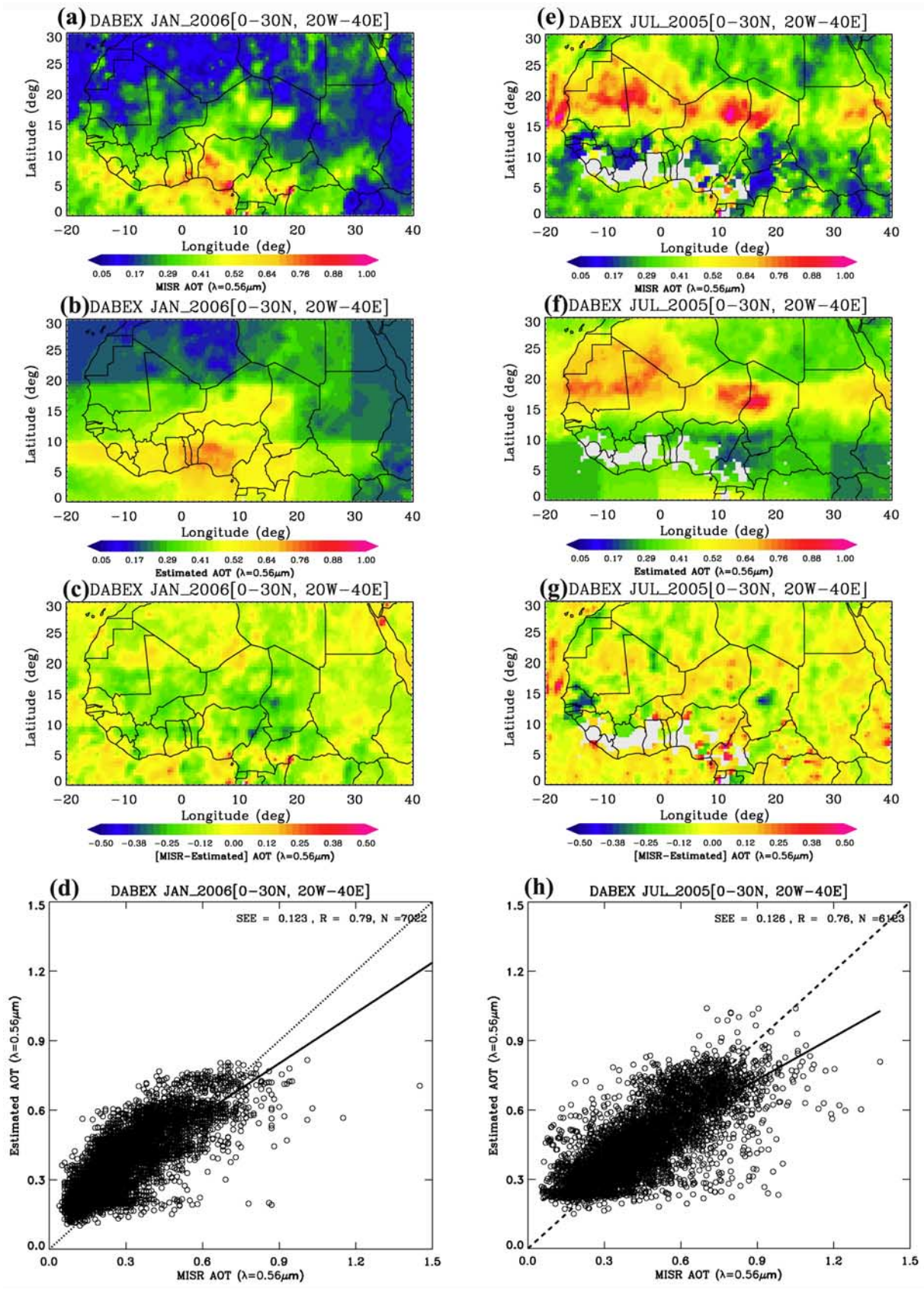

Figure 7. Spatial distribution of monthly mean MISR AOT and EAOT from the AI-AOT relationship for January 2006 and July 2005. (a and e) MISR AOT for January and July, (b and f) EAOTs for January and July, (c and g) the difference between MISR and EAOTs, and (d and h) the scatterplots between predicted EAOT and actual MISR AOT for January and July.

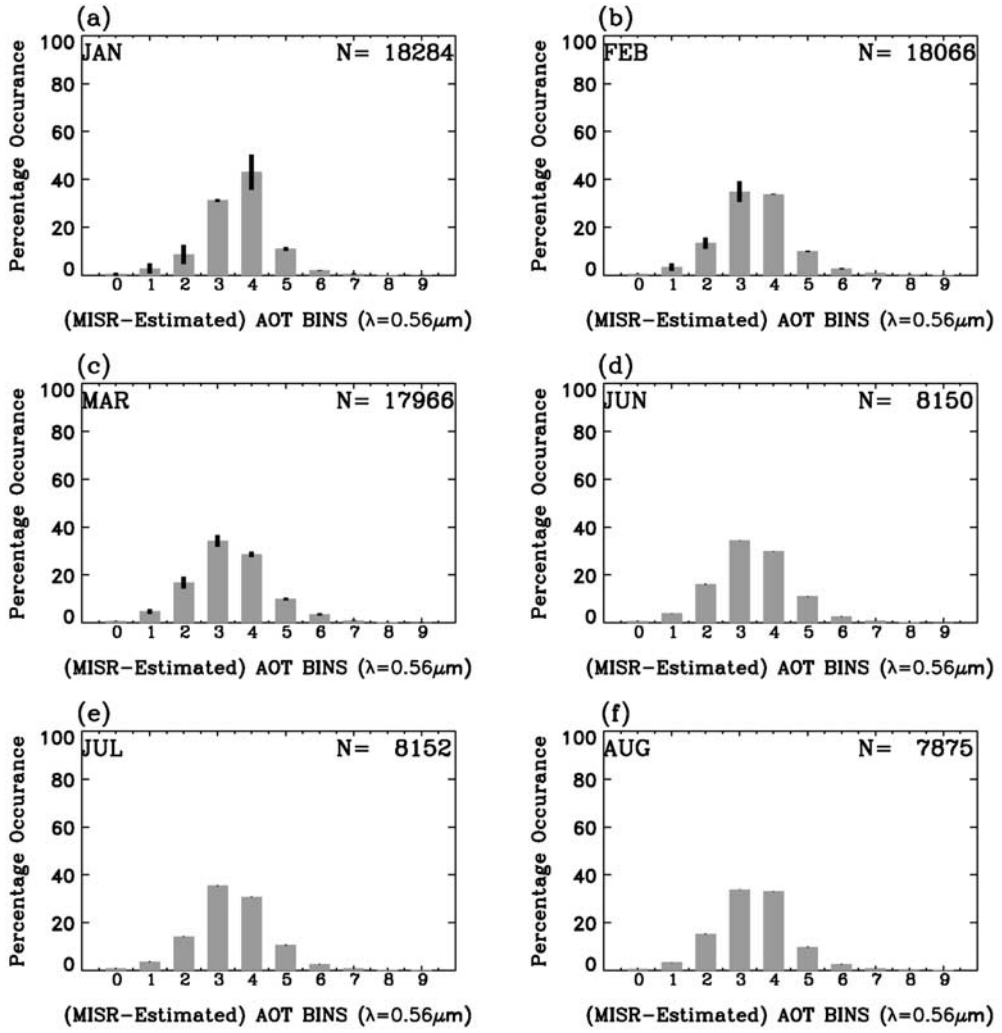

Bins	0	1	2	3	4	5	6	7	8	9
AOT Range	-0.5: - 0.4	-0.4: -0.3	-0.3: -0.2	-0.2: -0.1	-0.1: 0.0	0.0: 0.1	0.1: 0.2	0.2: 0.3	0.3: 0.4	0.4: 0.5

Figure 8. Composite results of the frequency distribution of MISR minus EAOT seasonal means from 2005 to 2006 for (a) January, (b) February, (c) March, (d) June, (e) July, and (f) August.

elevated layers of dust when compared to the spring months because of shallow boundary layer in the spring relative to summer.

[22] Overall, the AI-AOT relationship is more robust during JJA when compared to JFM. Correlation coefficient varies from low negative values to very high positive values (>0.9) over different years and grids. Over LLB, there is a very poor relationship between AI and AOT, especially during the dry season that could be due to a number of reasons including lack of elevated aerosols, subpixel cloud contamination and low concentrations of aerosols. Therefore, the AI-AOT relationship may not be appropriate for converting the AI to AOT values that is also a limitation of this method. Depending on the strength of dust storm or intensity of biomass burning, the aerosol height can change from year to year and hence the AI-AOT relationship changes. Correlation coefficients are consistently high during JJA in the MLB and ULB indicating the robustness of the AI-AOT relationship during months dominated by dust aerosols.

[23] Finally, mean linear regression equations for each season and for each grid box are derived using all the data. Figure 6 provides the 7 year mean of slope (m), intercept (c), correlation (r), and standard error of estimates (s) for each grid and for two seasons that could be used to invert the daily AI to AOT values. Again, overall correlation is better during summer when compared to spring months. *Hsu et al.* [1999] also note that that the absolute error in AOT derived from AI-AOT (from AERONET) at 440 nm is less (±0.12 to ±0.19) during the summer months when compared to the winter months (0.26–0.33) over dusty regions. However, our analysis indicates that AI-AOT relationships are necessary as a function of space and time and relationships obtained from point locations (e.g., AERONET) may not be applicable over larger domains.

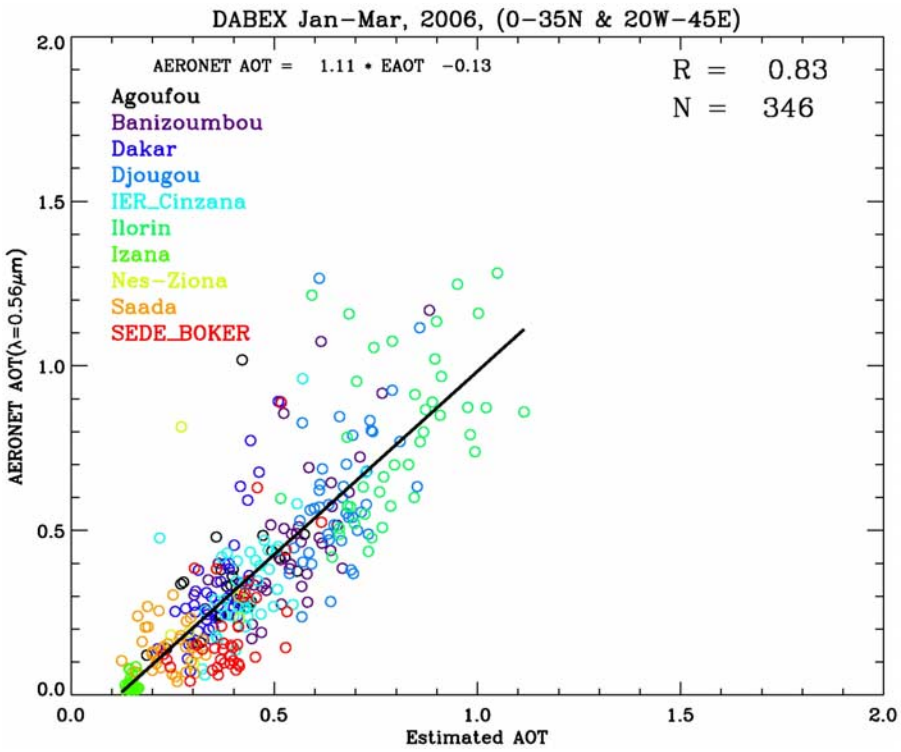

Figure 9. Intercomparison between hourly AERONET AOTs and EAOT over 10 different AERONET locations during January–March 2006.

[24] Figure 7 shows an example of the spatial distribution of the estimated AOT obtained from the 10° × 10° AI-AOT mean relationship (Figure 6) for January 2006 and July 2005. Figures 7a–7d is for January 2006 and Figures 7e–7h is for July 2005. Figure 7a is the monthly mean MISR AOT, Figure 7b is the EAOT from the AI-AOT relationship, Figure 7c is the difference between the MISR AOT and the EAOT (DAOT), and Figure 7d is the scatterplot of EAOT and the actual monthly mean MISR AOT. The spatial distribution of MISR and EAOT compares well for both January and July. The scatterplots shown in Figures 7e and 7h also shows that estimated values are underestimating AOTs where MISR has high AOT values. The scatterplot shows a good correlation with values greater than 0.75 for both months.

[25] Figure 8 presents composite results of the frequency distribution of the difference between the monthly mean MISR and EAOT during each month, averaged over a 2 year time period. Our results indicate that nearly 80% of the time, EAOT is higher by 0.2 or less compared to MISR AOTs. The frequency distribution of MISR minus EAOT does not show significant variations from one month to another. The MISR EAOT difference is between 0.0 and −0.1 for almost 35% of observations over all the months except during January when it is almost 50%. About 35–40% of the observations have differences between −0.1 and −0.2 and about 5–10 % falls within MISR EAOT values between 0.0 and 0.1. The number of data points in the ±0.2–0.3 bin is not significant. The percentage relative mean error (PRME) between EAOT and the actual MISR AOT was calculated as a function of six different AOT bins. This results indicate that the PRME could be as low as 18% for some seasons for moderate AOT range (0.4–0.8) with values close to 75% for small AOT value (<0.2). Averaged all the AOT bins, the overall mean PRME for all seasons and years is 28%. (Figure 9)

[26] Finally, we use the slope and intercepts derived using this method and estimate AOT during the time of the OMI overpass to compare against the AERONET AOT for JFM 2006 during DABEX. The OMI data were available over 10 different AERONET locations (Figure 1). The overall linear correlation between AERONET and the EAOT is 0.83 indicating the usefulness of this method. The relative mean error between these two data sets is 23%. This approach holds promise for obtaining AOTs at 0.55 μm from the AI-AOT relationships, and is complementary to other AOT products from MODIS and OMI. The OMI AI could therefore serve as a useful surrogate for obtaining AOT on a daily basis, an approach that has been adopted for intercomparison with high-resolution dust models [*Greed et al.*, 2008].

4. Summary and Conclusions

[27] In North Africa, there are several important aerosol sources including desert dust and smoke from biomass burning. While dust is predominant during the summer months (June–August), a combination of dust and smoke aerosols can be observed from satellite data during January–March. Currently there are several satellite sensors that provide information on dust and smoke spatial distribution and properties such as AOT. We combine the strengths of two satellite sensors (OMI and MISR) and develop an AOT product that can be used to verify numerical modeling results [e.g., *Haywood et al.*, 2005; *Greed et al.*, 2008]. Currently, the MISR is by far the best instrument to obtain

AOT values at 0.55 μm over deserts but it has a narrow swath width. The OMI provides absorbing AI values that are a measure of how smoke and dust absorbs in the Ultraviolet part of the EM spectrum. Since multisensor data offers a good solution to examine aerosol related issues, we investigated whether AI from the OMI instrument in the UV could be used as a surrogate for AOT. This is not a new approach since previous investigations have examined the AI-AOT relationship but over selected point AERONET locations. We therefore developed monthly mean, seasonal and region specific AI-AOT relationships from 2 years and then used these relationships to convert the AI to AOT values. To determine how robust these relationships are, we compared the estimated AOT with AERONET values over several locations during the DABEX field campaign. Our major conclusions are as follows:

[28] 1. The MISR continues to be an excellent tool for obtaining AOT over bright targets such as deserts as seen by the high correlations between MISR and AERONET AOT.

[29] 2. Although there is a large scatter due to sampling issues and vertical distribution of aerosols, as expected, there is indeed a linear relationship between AI-AOT indicating that the AI is a good surrogate for AOT.

[30] 3. However, when we examined the AI-AOT relationship in $10^\circ \times 10^\circ$ grids, our results showed that the AI-AOT relationship is region specific and is not robust over the entire study domain. It appears to work well during months when dust is prevalent closer to the source and also when the AOT and AI values are high.

[31] 4. The relationship is not as robust over smoke aerosol regions especially during low aerosol loadings and when biomass burning aerosols are closer to the boundary layer. Extreme caution should be used when using AI-AOT relationship during January–March, between 0 and 10°N.

[32] 5. Overall, applying the AI-AOT relationship to predict AOT values indicates that the OMI AI can estimate AOTs to within 28% for AOTs between 0.2 and 1.0 with much larger uncertainties for smaller AOTs.

[33] Finally, we note that the relationships that we have developed between AI-AOT are region specific and may not be applicable globally for other areas with dust aerosols. The slopes and intercepts provided in the paper can be used to convert the daily AI to AOT values.

[34] **Acknowledgments.** Sundar Christopher was supported by NASA's Radiation sciences, EOS, Interdisciplinary sciences, and ACMAP programs. Pawan Gupta was supported by NASA's Earth System Science Fellowship program for graduate students. The OMI data used in this study were acquired using the GES-DISC Interactive Online Visualization and Analysis Infrastructure (Giovanni) as part of the NASA's Goddard Earth Sciences (GES) Data and Information Services Center (DISC). The MISR data were obtained from Atmospheric Sciences Data Center at NASA Langley. We are thankful to the AERONET Principal Investigators for their efforts in establishing and maintaining these sites.

References

Andreae, M. O., and P. Merlet (2001), Emission of trace gases and aerosols from biomass burning, *Global Biogeochem. Cycles*, *15*(4), 955–966, doi:10.1029/2000GB001382.

Christopher, S. A., and J. Wang (2004), Intercomparison between MISR and Sunphotometer AOT in Dust Source Regions over China: Implication for satellite retrievals and radiative forcing calculations, *Tellus Ser. B*, *56*(5), 451–456, doi:10.1111/j.1600-0889.2004.00120.x.

Christopher, S. A., J. Wang, Q. Ji, and S.-C. Tsay (2003), Estimation of diurnal shortwave dust aerosol radiative forcing during PRIDE, *J. Geophys. Res.*, *108*(D19), 8596, doi:10.1029/2002JD002787.

de Graaf, M., P. Stammes, O. Torres, and R. B. A. Koelemeijer (2005), Absorbing Aerosol Index: Sensitivity analysis, application to GOME and comparison with TOMS, *J. Geophys. Res.*, *110*, D01201, doi:10.1029/2004JD005178.

Dubovik, O., and M. D. King (2000), A flexible inversion algorithm for retrieval of aerosol optical properties from Sun and sky radiance measurements, *J. Geophys. Res.*, *105*(D16), 20,673–20,696, doi:10.1029/2000JD900282.

Giglio, L., I. Csiszar, and C. O. Justice (2006), Global distribution and seasonality of active fires as observed with the Terra and Aqua Moderate Resolution Imaging Spectroradiometer (MODIS) sensors, *J. Geophys. Res.*, *111*, G02016, doi:10.1029/2005JG000142.

Greed, G., J. M. Haywood, S. Milton, A. Keil, S. Christopher, P. Gupta, and E. J. Highwood (2008), Aerosol optical thicknesses over North Africa: 2. Modeling and model validation, *J. Geophys. Res.*, *113*, D00C05, doi:10.1029/2007JD009457.

Haywood, J., et al. (2003), Radiative properties and direct radiative effect of Saharan dust measured by the C-130 aircraft during SHADE: 1. Solar spectrum, *J. Geophys. Res.*, *108*(D18), 8577, doi:10.1029/2002JD002687.

Haywood, J. M., et al. (2005), Can desert dust explain the outgoing longwave radiation anomaly over the Sahara during July 2003?, *J. Geophys. Res.*, *110*, D05105, doi:10.1029/2004JD005232.

Herman, J. R., P. K. Bhartia, O. Torres, C. Hsu, C. Seftor, and E. Celarier (1997), Global distribution of UV-absorbing aerosols from Nimbus 7/TOMS data, *J. Geophys. Res.*, *102*(D14), 16,911–16,922, doi:10.1029/96JD03680.

Holben, B. N., et al. (2001), An emerging ground-based aerosol climatology: Aerosol optical depth from AERONET, *J. Geophys. Res.*, *106*(D11), 12,067–12,097, doi:10.1029/2001JD900014.

Hsu, N. C., et al. (1999), Comparisons of the TOMS aerosol index with Sun-photometer aerosol optical thickness: Results and applications, *J. Geophys. Res.*, *104*(D6), 6269–6280, doi:10.1029/1998JD200086.

Hsu, N. C., J. R. Herman, and C. Weaver (2000), Determination of radiative forcing of Saharan dust using combined TOMS and ERBE data, *J. Geophys. Res.*, *105*(D16), 20,649–20,662, doi:10.1029/2000JD900150.

Hsu, N. C., S. C. Tsay, M. D. King, and J. R. Herman (2006), Deep blue retrievals of Asian aerosol properties during ACE-Asia, *IEEE Trans. Geosci. Remote Sens.*, *44*, 3180–3195, doi:10.1109/TGRS.2006.879540.

Intergovernmental Panel on Climate Change (2007), *Climate Change 2007: The Physical Science Basis, Contribution of Working Group I to the Fourth Assessment Report of the Intergovernmental Panel on Climate Change*, edited by S. Solomon et al., Cambridge Univ. Press, Cambridge, U. K.

Kahn, R. A., B. J. Gaitley, J. V. Martonchik, D. J. Diner, K. A. Crean, and B. Holben (2005), Multiangle Imaging Spectroradiometer (MISR) global aerosol optical depth validation based on 2 years of coincident Aerosol Robotic Network (AERONET) observations, *J. Geophys. Res.*, *110*, D10S04, doi:10.1029/2004JD004706.

Kiss, P., I. M. Jánosi, and O. Torres (2007), Early calibration problems detected in TOMS Earth-Probe aerosol signal, *Geophys. Res. Lett.*, *34*, L07803, doi:10.1029/2006GL028108.

Mahowald, N. M., and J. L. Dufresne (2004), Sensitivity of TOMS aerosol index to boundary layer height: Implications for detection of mineral aerosol sources, *Geophys. Res. Lett.*, *31*, L03103, doi:10.1029/2003GL018865.

Martonchik, J. V., et al. (1998), Techniques for the retrieval of aerosol properties over land and ocean using multiangle imaging, *IEEE Trans. Geosci. Remote Sens.*, *36*, 1212–1227, doi:10.1109/36.701027.

Mishchenko, M., et al. (2004), Monitoring of aerosol forcing of climate from space: Analysis of measurement requirements, *J. Quant. Spectrosc. Radiat. Transfer*, *88*, 149–161, doi:10.1016/j.jqsrt.2004.03.030.

Osborne, S. R., B. Johnson, and J. Haywood (2008), Physical and optical properties of mineral dust aerosol during the Dust and Biomass Experiment (DABEX), *J. Geophys. Res.*, doi:10.1029/2007JD009551, in press.

Prospero, J. M., P. Ginoux, O. Torres, S. Nicholson, and T. E. Gill (2002), Environmental characterization of global sources of atmospheric soil dust identified with the NIMBUS-7 Total Ozone Mapping Spectrometer (TOMS) absorbing aerosol product, *Rev. Geophys.*, *40*(1), 1002, doi:10.1029/2000RG000095.

Remer, L. A., et al. (2005), The MODIS aerosol algorithm, product, and validation, *J. Atmos. Sci.*, *62*, 947–973, doi:10.1175/JAS3385.1.

Stephens, G. L., et al. (2005), The CloudSat mission and the A-train: A new dimension of space-based observations of clouds and precipitation, *Bull. Am. Meteorol. Soc.*, *83*, 1771–1790, doi:10.1175/BAMS-83-12-1771.

Swap, R. J., et al. (2003), Africa burning: A thematic analysis of the Southern African Regional Science Initiative (SAFARI 2000), *J. Geophys. Res.*, *108*(D13), 8465, doi:10.1029/2003JD003747.

Tanré, D., et al. (2003), Measurement and modeling of the Saharan dust radiative impact: Overview of the Saharan Dust Experiment (SHADE), *J. Geophys. Res.*, *108*(D18), 8574, doi:10.1029/2002JD003273.

Torres, O., P. K. Bhartia, J. R. Herman, and Z. Ahmad (1998), Derivation of aerosol properties from satellite measurements of backscattered ultraviolet radiation: Theoretical basis, *J. Geophys. Res.*, *103*, 17,099–17,110, doi:10.1029/98JD00900.

Torres, O., P. K. Bhartia, J. R. Herman, A. Sinyuk, and B. Holben (2002), A long term record of aerosol optical thickness from TOMS observations and comparison to AERONET measurements, *J. Atmos. Sci.*, *59*, 398–413, doi:10.1175/1520-0469(2002)059<0398:ALTROA>2.0.CO;2.

Torres, O., P. K. Bhartia, A. Sinyuk, E. J. Welton, and B. Holben (2005), Total Ozone Mapping Spectrometer measurements of aerosol absorption from space: Comparison to SAFARI 2000 ground-based observations, *J. Geophys. Res.*, *110*, D10S18, doi:10.1029/2004JD004611.

Torres, O., A. Tanskanen, B. Veihelmann, C. Ahn, R. Braak, P. K. Bhartia, P. Veefkind, and P. Levelt (2007), Aerosols and surface UV products from Ozone Monitoring Instrument observations: An overview, *J. Geophys. Res.*, *112*, D24S47, doi:10.1029/2007JD008809.

Wang, J., X. Xia, P. Wang, and S. A. Christopher (2004), Diurnal variability of dust aerosol optical thickness and Angstrom exponent over dust source regions in China, *Geophys. Res. Lett.*, *31*, L08107, doi:10.1029/2004GL019580.

Zhang, J., and S. A. Christopher (2003), Longwave radiative forcing of Saharan dust aerosols estimated during MODIS, MISR, and CERES observations on Terra, *Geophys. Res. Lett.*, *30*(23), 2188, doi:10.1029/2003GL018479.

S. A. Christopher and P. Gupta, Department of Atmospheric Sciences, University of Alabama in Huntsville, 320 Sparkman Drive, Huntsville, AL 35806, USA. (sundar@nsstc.uah.edu)

J. Haywood and G. Greed, United Kingdom Meteorological Office, FitzRoy Road, Devon, EX1 3PB, UK.